THE JOURNAL OF PHYSICAL CHEMISTRY C

Article

pubs.acs.org/JPCC

Enhancing Dissociative Adsorption of Water on Cu(111) via Chemisorbed Oxygen

Qianqian Liu,[†] Jonathan Li,[‡] Xiao Tong,[§] and Guangwen Zhou*[,†]

[†]Department of Mechanical Engineering & Materials Science and Engineering Program, State University of New York, Binghamton, New York 13902, United States

[‡]Department of Physics, Applied Physics and Astronomy & Materials Science and Engineering Program, State University of New York, Binghamton, New York 13902, United States

[§]Center for Functional Nanomaterials, Brookhaven National Laboratory, Upton, New York 11973, United States

Supporting Information

ABSTRACT: We have used X-ray photoelectron spectroscopy to study the dehydrogenation of H_2O molecules on the clean and oxygenated Cu(111) surfaces. The clean surface does not show reactivity toward H_2O dehydrogenation. By contrast, H_2O molecules on the oxygenated Cu(111) dissociate into OH species by reacting with chemisorbed oxygen until the complete consumption of the chemisorbed oxygen at which the surface loses its reactivity toward H_2O dehydrogenation. Increasing the temperature to 200 °C and above decreases molecularly adsorbed H_2O for dehydrogenation, thereby resulting in less loss of chemisorbed O. In conjunction with density-functional theory calculations, a three-step reaction pathway is proposed to account for the chemisorbed O assisted dehydrogenation of H_2O molecules and the net loss of surface oxygen. These results provide insight into understanding the elemental steps of the dehydrogenation of H_2O molecules and the controllable conditions for tuning H_2O dissociation on metal surfaces.

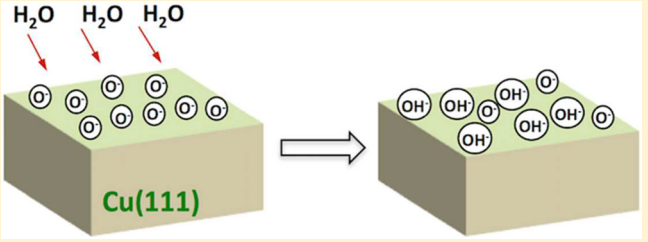

1. INTRODUCTION

The catalytic properties of metal catalysts can be altered by the introduction of a small amount of impurities that can speed up or slow down certain reaction steps. Surface oxygen has been shown to play such a role in influencing the dehydrogenation reactions catalyzed by transitional metals.[1−5] However, discrepancies remain regarding the effect of surface oxygen either as a promoter or poison. For example, it is generally believed that the formation of strong chemisorbed atomic oxygen poisons the active surface sites and thus inhibits dehydrogenation reactions.[3,4] However, it has been also shown that surface oxygen can strongly activate the oxygen-, carbon-, sulfur-, and nitrogen−hydrogen bonds and thus promote the dehydrogenation reactions.[6−11]

Many studies have been conducted to identify the role that preadsorbed oxygen atoms play on H_2O adsorption and dissociation on various transitional metal surfaces.[12−15] DFT calculations showed that preadsorbed oxygen atoms strengthen the adsorption of H_2O and lower the energy barrier of H_2O dissociation compared to the clean surfaces of Al(111),[12] Au(100),[13] Fe(100),[14] and Cu surfaces.[15] These modeling results indicate that the adsorption energy of preadsorbed oxygen atoms as well as the distance between the preadsorbed oxygen atom and H_2O molecule plays significant roles in the promotion effect. The preadsorbed oxygen may form a hydrogen bond with an H atom of the H_2O molecule. When the distance between the preadsorbed oxygen atom and H_2O molecule is shorter, the stronger the promotion effect is. The more strongly the oxygen atom binds to the metal surface, the less promotion effect it has on H_2O dissociation.

The dehydrogenation reactions at metal surfaces are relevant to a wide variety of catalytic processes. Good examples include the water−gas-shift reaction (WGS) ($H_2O + CO = H_2 + CO_2$) and steam reforming (SR) ($CH_4 + H_2O = CO + 3H_2$) for massive H_2 production based on Cu catalysts, both of which are cornerstones of today's large-scale chemical industry and form the basis for ammonia and methanol synthesis. In low-temperature WGS catalyzed by Cu, for example, the dissociative adsorption of H_2O has been identified as a rate-limiting step.[16−19] This has therefore motivated much interest for understanding the fundamental interactions involved in the H_2O−Cu system. Recent developments in this area involve X-ray photoelectron spectroscopy (XPS) investigations under near-ambient conditions of water vapor pressure, which showed that H_2O dissociates on Cu(110) via an autocatalytic process enabled by the formation of stable H_2O−OH complexes, by contrast, H_2O does not dissociate on the Cu(111) surface under the identical condition (e.g., 1 Torr of H_2O vapor pressure).[20] The difference in H_2O dissociation for the two Cu surfaces is attributed to the different activation barriers for OH

Received: December 22, 2016
Revised: May 16, 2017
Published: May 16, 2017

ACS Publications © 2017 American Chemical Society

DOI: 10.1021/acs.jpcc.6b12897
J. Phys. Chem. C 2017, 121, 12117−12126

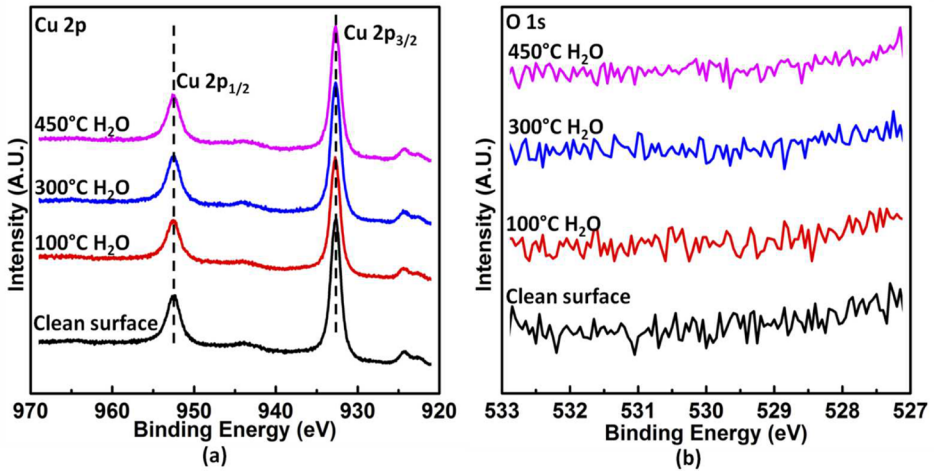

Figure 1. Photoemission spectra of the Cu 2p (a) and O 1s (b) region for a freshly cleaned Cu(111) surface and its exposure to $p(H_2O) = 1 \times 10^{-5}$ Torr for 60 min at T = 100, 300, and 450 °C, respectively.

formation, i.e., a lower H_2O dissociation barrier on Cu(110) than Cu(111). The dissociation barriers have been determined experimentally by near ambient pressure kinetic measurements in a micro reactor to be 0.87 eV[17] and 1.17 eV[21] for Cu(110) and Cu(111), respectively.

Similar ambient-pressure XPS experiments have shown the presence of absorbed oxygen can make the Cu(111) surface hydrophilic.[20] This happens because the absorbed oxygen induces H_2O dissociation into OH groups that stabilize water molecules on the surface via forming strongly bound H_2O−OH complexes. These results have demonstrated that the presence of OH species can facilitate the dehydrogenation reaction by anchoring H_2O molecules on the surface but also raise some questions: How do H_2O molecules interact with the chemisorbed oxygen to form OH species? How stable are adsorbed OH species? What is the chemical state of the metal atoms at the surface? With the aim of developing basic insight into these questions and understanding the fundamental interactions involved in the H_2O−Cu system, we conduct a comparative study of the interaction of H_2O with clean and oxygenated Cu(111) at temperatures varying from 100 to 450 °C. Using XPS, the temporal evolution of adsorbed surface species of O and OH during H_2O exposure at the different temperatures is determined. Detailed analysis of the spectral features and binding energies reveal that the H_2O dehydrogenation reaction requires consumption of adsorbed oxygen, which results in the gradual loss of the surface activity toward H_2O dissociation.

2. EXPERIMENTAL AND COMPUTATIONAL METHODS

The experiments were performed in an ultrahigh vacuum (UHV) system with a base pressure of ~1×10^{-9} Torr. The system is equipped with an XPS SPECS Phoibos 100, MCD-5 electron analyzer and an Ar-ion sputtering gun. A non-monochromatized Mg Kα X-ray source ($h\nu$ = 1253.6 eV) with the electron energy analyzer operated at 10 kV anode voltage and 30 mA emission current was used for the XPS studies. The Cu(111) single crystal (Princeton Scientific Corp., purity: 99.9999%) is a top-hat shaped disc (1 mm in thickness and 8 mm in diameter), cut to within 0.1° of the (111) crystallographic orientation and polished to a mirror finish. The sample was heated via a ceramic button heater, and its temperature was monitored with a type-K thermocouple. The Cu(111) surface was cleaned by repeated cycles of Ar^+ bombardment (2×10^{-5} Torr of Ar gas, 2.8 μA cm^{-2}, 1.5 keV) at room temperature followed by annealing at 600 °C for 10 min until no O and C spectra could be detected by XPS. The XPS detection angle θ between the axis of the photoelectron analyzer and the normal to the sample surface was set at 0° in our geometry.

Oxygen gas (purity = 99.9999%) was directly introduced to the system through a variable-pressure leak valve to form a chemisorbed oxygen layer on the Cu(111) surface before water vapor dosing. To perform water vapor exposure, water (18.2 MΩ) was put into a flask and purified with several freeze−pump−thaw cycles before dosing through a variable-pressure leak valve separate from the one for O_2 dosing. An ion gauge was used to measure the gas pressure in the chamber. The effect of the ion gauge sensitivity correction was not accounted during the pressure measurements due to the minor difference in the gas correction factors for O_2 and H_2O (O_2 = 1.01 and H_2O = 1.12 relative to N_2 = 1.00). XPS measurements showed that the freshly cleaned Cu(111) and the surface after O_2 and H_2O exposure remain free of carbon contamination (see the Supporting Information).

First, the freshly cleaned Cu(111) surface was exposed to $p(H_2O) = 1 \times 10^{-5}$ Torr at T = 100, 300, and 450 °C, respectively. Cu 2p and O 1s XPS spectra were obtained to monitor the surface species and chemical state right after the H_2O exposure. Then the freshly cleaned Cu(111) surface was first exposed to $p(O_2) = 1 \times 10^{-5}$ Torr at 400 °C for 60 min to form a chemisorbed layer of oxygen. Oxygen dosing under this condition results in ordered "29" ($\sqrt{13}R46.1° \times 7R21.8°$), and "44" ($\sqrt{73}R5.8° \times \sqrt{21}R10.9°$) reconstructions, as shown previously[22−26] and also confirmed by our own scanning tunneling microscopy (STM) imaging. These structures comprise hexagonal arrays of chemisorbed O atoms arranged in parallel lines in the first layer, with the unit cell areas 29 and 44 times larger than that of the substrate Cu(111). After being confirmed by XPS, the oxygenated Cu(111) surface was exposed to water vapor at T = 100, 200, 300, and 450 °C, respectively. To obtain a clear trend of the reaction behavior, three water vapor pressures were examined for each temperature: $p(H_2O) = 1 \times 10^{-7}$, 1×10^{-6}, and 1×10^{-5} Torr. Cu 2p and O 1s XPS spectra and Cu LMM X-ray excited Auger electron spectra (XAES) were obtained to monitor the surface

DOI: 10.1021/acs.jpcc.6b12897
J. Phys. Chem. C 2017, 121, 12117−12126

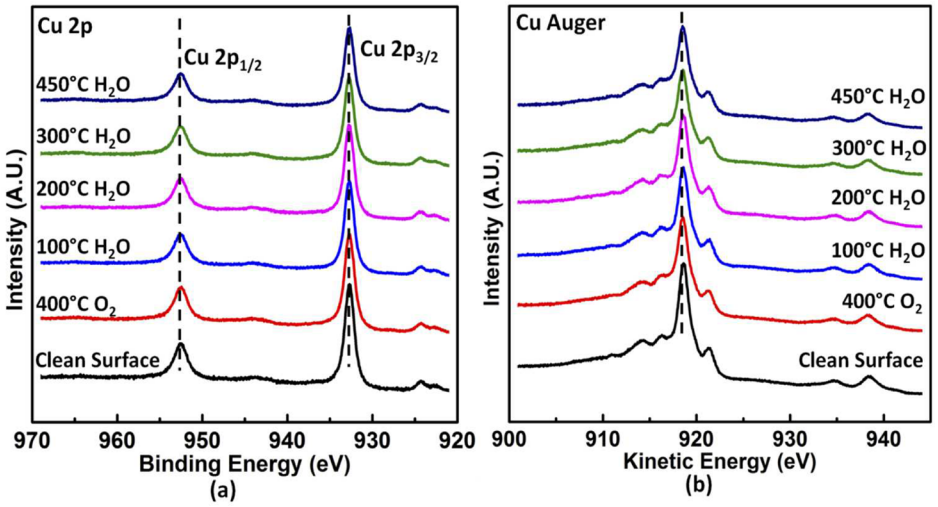

Figure 2. Photoemission spectra of the Cu 2p (a) and Cu LMM (b) region from the freshly cleaned Cu(111) surface, and after its exposure to $p(O_2) = 1 \times 10^{-5}$ Torr for 60 min at 400 °C, followed by exposure to $p(H_2O) = 1 \times 10^{-7}$ Torr until reaching a steady state at T = 100, 200, 300, and 450 °C, respectively.

species and chemical state right after each O_2 and H_2O exposure. To minimize the chance of the measurement errors (including temperature effect on the intensity attenuation) and obtain sufficiently reliable XPS data for quantification, all of the XPS and XAES were acquired at room temperature and under UHV condition. Meanwhile, all of the XPS data acquisition parameters were kept constant including the geometry of the X-ray gun, sample, and analyzer. Also, the surface coverage was obtained by measuring the relative O 1s and Cu 2p regions and calibrating against the saturated oxygen coverage (~0.50 monolayer, ML) of the "29" or "44" structure.[22−24,26]

The DFT calculations were performed using the Vienna ab initio simulation package (VASP)[27,28] with the PW91 generalized gradient approximation (GGA)[29] and projector augmented wave (PAW)[30,31] potentials. We have performed both spin and nonspin polarized calculation tests to ensure that the spin did not have an effect in describing the transition state and found that there was no significant difference in the results. The Brillouin-zone integration was performed using (4 × 4 × 1) K-point meshes based on Monkhorst−Pack grids[32] and with broadening of the Fermi surface according to Methfessel-Paxton smearing technique with a smearing parameter of 0.2 eV. We calculated the lattice constant of Cu to be 3.64 Å, consistent with previous work.[33−36] The Cu(111) surface was simulated by a four-layer 4 × 4 slab model. The bottom two layers of the Cu surface were fixed at the lattice position, and all other atoms were allowed to fully relax during optimization until all force components acting on the atoms are below 0.02 eV/Å. Successive slabs are separated by a vacuum region of 12 Å. We applied the climbing image nudged elastic bands (CI-NEB) method[37] to calculate the reaction barriers, where we used five intermediate images between the initial and final states. The atomic structures are visualized using the VESTA package.[38]

3. RESULTS

The dissociation of water molecules on clean and oxygenated Cu(111) surfaces was comparatively studied by XPS. Figure 1a shows typical XPS spectra of the Cu 2p peaks obtained from the freshly cleaned Cu(111) surface and subsequent exposure to $p(H_2O) = 1 \times 10^{-5}$ Torr for 60 min at T = 100 °C, 300 °C, and 450 °C, respectively. The shape and position of the Cu 2p core level peaks (binding energies (BE) = 952.3 and 932.6 eV) remain all the same for the clean and H_2O exposed Cu(111) surfaces, indicating that Cu is not oxidized and remains its metallic state after the H_2O exposure at the different temperatures. In addition, the intensity of the Cu 2p peaks for the H_2O exposed surfaces remains nearly the same as the clean Cu(111) surface, suggesting that the H_2O exposure does not result in any adsorbed species on the Cu(111) surface. The lack of the surface activity toward H_2O dissociation is also confirmed by XPS O 1s spectra obtained from the H_2O exposed surfaces, as shown in Figure 1b. Same as the clean surface, there is no detectable intensity of the O 1s spectra after the H_2O exposure. These XPS measurements confirm that H_2O does not dissociate on the clean Cu(111) surface under the conditions of the vapor pressure and temperatures examined here.

We then examined the activity of the oxygenated Cu(111) surface toward H_2O dissociation. Figure 2a shows the XPS spectra of the Cu 2p peaks obtained from the Cu(111) surface that is first exposed to $p(O_2) = 1 \times 10^{-5}$ Torr at T = 400 °C for 60 min to form a saturated chemisorbed oxygen layer, followed by exposure to $p(H_2O) = 1 \times 10^{-7}$ Torr at T = 100, 200, 300, and 450 °C, respectively, until the surface reaches a steady state at each temperature (note that a freshly formed oxygenated Cu(111) surface is used for each H_2O exposure at the different temperatures). The Cu 2p peaks located at BE = 952.3 and 932.6 eV correspond to the metallic Cu and they remain the same after the oxygen exposure at $p(O_2) = 1 \times 10^{-5}$ Torr and T = 400 °C. The subsequent H_2O exposure of the oxygenated Cu(111) surface to $p(H_2O) = 1 \times 10^{-7}$ Torr at the different temperatures results in no changes in the shape and position of the Cu 2p peaks. Similarly, no noticeable changes are observed in the Cu 2p peaks from the exposure of the oxygenated Cu(111) surface to $p(H_2O) = 1 \times 10^{-6}$ and 1×10^{-5} Torr, respectively.

Cu 2p XPS spectra can differentiate between metallic Cu (Cu^0) and Cu^{2+} but cannot distinguish between Cu^0 and Cu^+ because their binding energies are very close. Peak positions and line shapes of XAES have proved to be sensitive enough for Cu oxidation state analysis for providing more unambiguous

DOI: 10.1021/acs.jpcc.6b12897
J. Phys. Chem. C 2017, 121, 12117−12126

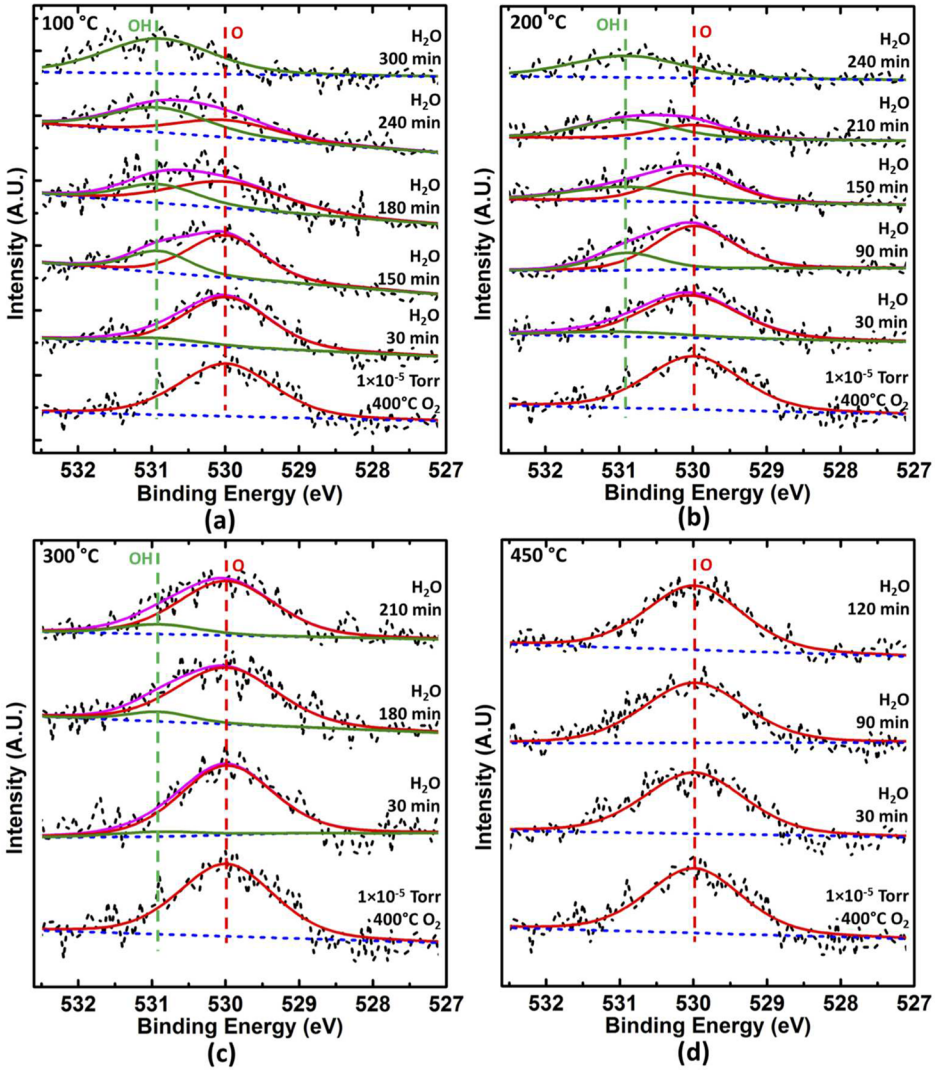

Figure 3. Photoemission spectra of the O 1s region for the exposure of the oxygenated Cu(111) to $p(H_2O) = 1 \times 10^{-7}$ Torr at (a) 100, (b) 200, (c) 300, and (d) 450 °C, respectively, until reaching the steady state.

differences between Cu^0 and Cu^+ than Cu 2p XPS core level shifts.[39,40] Therefore, XAES of the Cu LMM peaks are also acquired to further confirm the valence states of Cu, as shown in Figure 2b. The clean Cu(111) surface shows the Cu LMM line peak at a kinetic energy of 918.6 eV, which is associated with metallic Cu^0. The O_2 exposure at $p(O_2) = 1 \times 10^{-5}$ Torr and T = 400 °C and the subsequent H_2O exposures at the different vapor pressures and temperatures result in no changes in the line position and shape of the Cu LMM spectra. These combined XPS and XAES measurements demonstrate that the Cu(111) surface still maintains its metallic state (Cu^0) although the surface is covered with chemisorbed O and OH species as shown below. It should be noted that at higher temperatures there is a small intensity loss of Cu 2p XPS peak and Cu LMM Auger peak in Figure 2 for unknown reasons.

O 1s spectra are also obtained from the Cu(111) surface exposed to O_2 and subsequently to H_2O. Figure 3 illustrates the evolution of the O 1s core level region, where the freshly cleaned Cu(111) surface is first exposed to $p(O_2) = 1 \times 10^{-5}$ Torr and T = 400 °C to form a chemisorbed oxygen layer prior to the H_2O exposure. It can be seen that the O_2 exposure results in appreciable intensity in the O 1s core level centered at BE = 530.0 eV. This is completely different from the H_2O exposure to the clean Cu(111) surface, where no detectable O 1s spectra are observed (Figure 1). Since Cu is in the metallic state as shown in Figure 2, the O 1s intensity is related to the chemisorbed oxygen on the Cu(111) surface.

Figure 3a corresponds to the evolution of the O 1s spectra from the exposure of the oxygenated Cu(111) to $p(H_2O) = 1 \times 10^{-7}$ Torr at 100 °C. The O 1s peak gradually shifts to higher BE and becomes broader and asymmetrical with a shoulder on the high BE side. Using the same fitting parameters for the chemisorbed O does not provide an overall good fitting to the O 1s peak after the H_2O exposure, and a second peak at the higher BE arises. The spectra are deconvoluted into two peaks with BE = 530.0 and 530.9 eV, respectively. The peak at 530.0 eV is associated with the chemisorbed O, and the other peak at BE = 530.9 eV is attributed to the O in adsorbed OH species, which is in good agreement with the literature value. H_2O exposure under the near ambient pressure of 1 Torr has been shown to result in molecular H_2O adsorption that produces a peak in the 532.4−533.0 eV range.[20] In contrast, no stable molecular H_2O adsorption occurs on the oxygenated Cu(111) surface exposed to the low H_2O pressure shown here. As seen in Figure 3a, the OH peak increases while the chemisorbed O peak decreases in intensity as the H_2O exposure continues. The

DOI: 10.1021/acs.jpcc.6b12897
J. Phys. Chem. C 2017, 121, 12117−12126

Table 1. Binding Energies (eV) of O (1s) and OH Spectra at the Steady State from the H_2O Exposure of the Oxygenated Cu(111)

	water vapor exposure temperature							
	100 °C		200 °C		300 °C		450 °C	
water vapor pressure (Torr)	O 1s	OH	O 1s	OH	O 1s	OH	O 1s	OH
1×10^{-7}		530.9		530.9	530.0	530.9	530.0	
1×10^{-6}		530.9		530.9	530.0	530.9	530.0	
1×10^{-5}		530.9		530.9	530.0	530.9	530.0	530.9

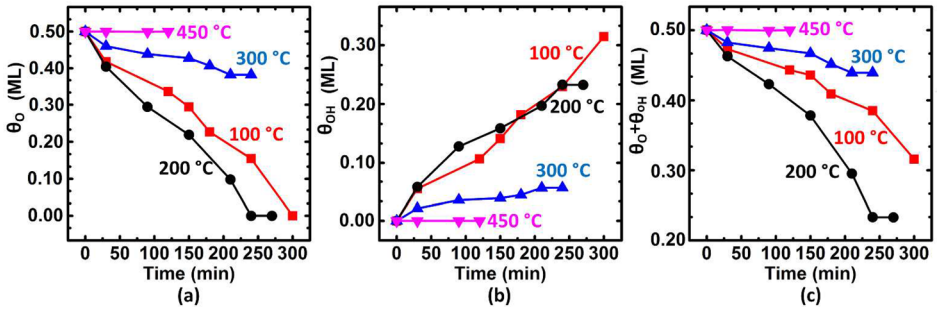

Figure 4. Evolution of the surface coverage of chemisorbed O (a), OH species (b), and total oxygen-containing components (both chemisorbed O and OH) (c) upon the exposure of the oxygenated Cu(111) surface to $p(H_2O) = 1 \times 10^{-7}$ Torr at the different temperatures.

chemisorbed O peak disappears completely after ~300 min of H_2O exposure, beyond which further H_2O exposure does not lead to any noticeable changes in the collected Cu 2p, Cu LMM and O 1s spectra including peak positions and intensities. This indicates that the dissociation of H_2O molecules requires the consumption of chemisorbed O and the surface gradually loses its activity to H_2O dissociation as the amount of chemisorbed O decreases. It can be also noted that the overall intensity of the O 1s spectra decreases after the surface becomes completely inert toward H_2O dissociation.

Figure 3b shows the evolution of the O 1s spectra from the exposure of a freshly prepared oxygenated Cu(111) to $p(H_2O) = 1 \times 10^{-7}$ Torr at T = 200 °C. Similarly, the H_2O exposure results in an OH peak with BE = 530.9 eV in addition to the chemisorbed O peak at BE = 530.0 eV. After ~210 min of H_2O exposure, the chemisorbed O peak still remains in the same position of BE = 530.0 eV but its intensity drops significantly. Meanwhile, the OH peak intensity increases slightly. The chemisorbed O peak disappears completely after ~240 min of H_2O exposure, and the OH peak is stabilized at BE = 530.9 eV with further H_2O exposure, indicating that the surface becomes nonreactive toward further H_2O dissociation.

Figure 3c shows the O 1s spectra of the oxygenated Cu(111) surface exposed to $p(H_2O) = 1 \times 10^{-7}$ Torr at T = 300 °C. Similarly, the O 1s spectra obtained after ~30 min of H_2O exposure can be deconvoluted into the chemisorbed O peak with BE = 530.0 eV and the OH peak with BE = 530.9 eV. The surface reaches its steady state after ~210 min of the H_2O exposure, where both the chemisorbed O and OH peaks are present although the OH peak is much weaker. This is different from the steady state of the H_2O exposure at 100 and 200 °C as shown in Figure 3a,b, where the O peak disappears completely. Such a temperature effect on the evolution of the relative intensity of the chemisorbed O and OH peaks is further evident from H_2O exposure at 450 °C, for which the chemisorbed O peak does not show any appreciable changes throughout the H_2O dosing process and only the chemisorbed O peak (BE = 530.0 eV) is present (Figure 3d).

The temperature effect on the dissociation of water molecules on the oxygenated Cu(111) surface is also examined for H_2O exposure at $p(H_2O) = 1 \times 10^{-6}$ and 1×10^{-5} Torr. Table 1 summarizes the positions of the chemisorbed O and OH peaks at the steady state of the surface for all three water vapor pressures examined at T = 100, 200, 300, and 450 °C. The positions of the chemisorbed O and OH peaks are constant. The chemisorbed O peak disappears completely for H_2O exposure at 100 and 200 °C for all three vapor pressures. H_2O exposure at 300 °C results in a weak OH peak in addition to the dominant chemisorbed O peak for all three vapor pressures. The H_2O exposure at 450 °C results in only the chemisorbed O peak for $p(H_2O) = 1 \times 10^{-7}$ Torr and $p(H_2O) = 1 \times 10^{-6}$ Torr while both the chemisorbed O and OH peaks are observed for $p(H_2O) = 1 \times 10^{-5}$ Torr.

Figure 4 shows the evolution of the intensity ratio for chemisorbed O, OH, and their total (O + OH) to the Cu 2p peak at $p(H_2O) = 1 \times 10^{-7}$ Torr and the different temperatures. The first point (i.e., t = 0 min) in each plot corresponds to the freshly prepared "29" or "44" oxygenated Cu(111) before H_2O exposure. As shown in Figure 4a, chemisorbed O gradually decreases with time for H_2O exposure at $T \leq 300$ °C and chemisorbed O remains unchanged for H_2O exposure at T = 450 °C. Figure 4b shows that OH gradually increases with time for H_2O exposure at $T \leq 300$ °C, and no OH formation at 450 °C. It can be also noted that OH at the steady state decreases as the H_2O exposure temperature increases. The total amount of the oxygen containing components (O and OH) gradually decreases over time (Figure 4c), indicating that the loss of chemisorbed O is more than the formation of OH species (there is only chemisorbed O at 450 °C because of the lack of OH formation at this temperature). This suggests that the formation of adsorbed OH species is accompanied by the concomitant removal of chemisorbed O from the surface. It is noticeable that chemisorbed O drops to zero after 300 min of H_2O exposure at 100 °C and after 240 min of H_2O exposure at 200 °C, beyond which no further OH formation occurs. This indicates

DOI: 10.1021/acs.jpcc.6b12897
J. Phys. Chem. C 2017, 121, 12117−12126

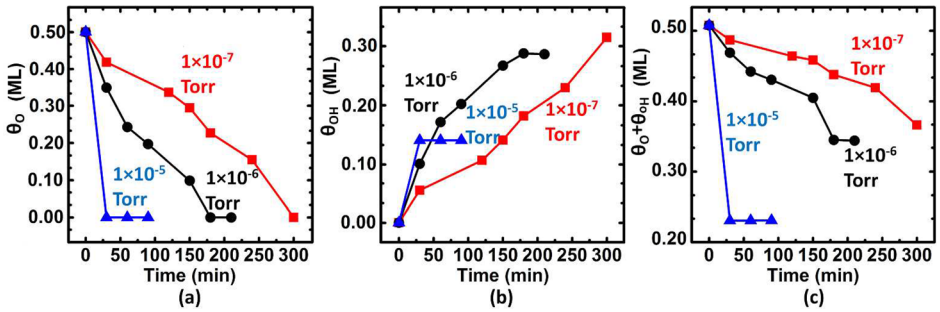

Figure 5. Evolution of the surface coverage of chemisorbed O (a), OH species (b), and the total (both O and OH) (c) after reaching the steady state from the exposure of the oxygenated Cu(111) surface to water vapor at 100 °C and three different vapor pressures.

Table 2. Surface Coverage (ML) of Chemisorbed O (θ_O) and OH (θ_{OH}) at the Steady State from the H_2O Exposure of the Oxygenated Cu(111)

	water vapor exposure temperature							
	100 °C		200 °C		300 °C		450 °C	
water vapor pressure (Torr)	θ_O	θ_{OH}	θ_O	θ_{OH}	θ_O	θ_{OH}	θ_O	θ_{OH}
1×10^{-7}	0	0.316	0	0.233	0.393	0.056	0.500	0
1×10^{-6}	0	0.287	0	0.221	0.385	0.051	0.500	0
1×10^{-5}	0	0.140	0	0.129	0.308	0.047	0.500	0.04

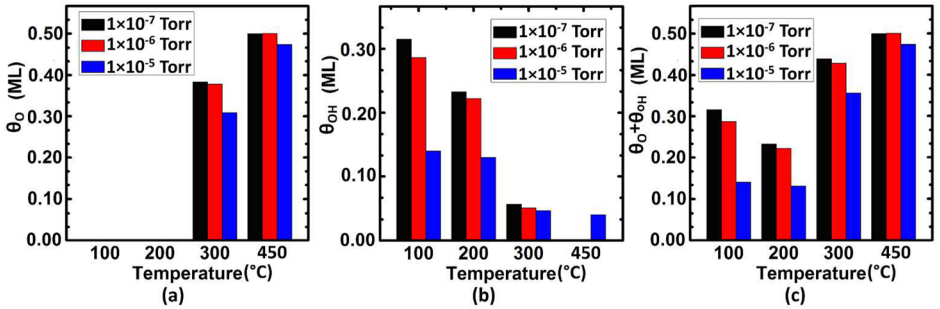

Figure 6. Temperature and pressure dependence of the surface coverage of chemisorbed O (a), OH (b), and total (both O and OH) (c) after reaching the steady state from the H_2O exposure of the oxygenated Cu(111).

that the prechemisorbed O is required for dissociative adsorption of H_2O molecules. For H_2O exposure at T = 300 °C, chemisorbed O does not drop to zero at the steady state. For H_2O exposure at T = 450 °C, there is neither OH formation nor O loss, indicating that H_2O does not dissociate under this condition.

The temperature effect on H_2O dissociation is also examined at $p(H_2O) = 1 \times 10^{-6}$ and 1×10^{-5} Torr. Chemisorbed O is completely consumed after reaching the steady state for H_2O exposure at T = 100 or 200 °C. For H_2O exposure at 300 °C, only a small amount of chemisorbed O is consumed. However, for H_2O exposure at 450 °C, the steady-state surface species depend on the vapor pressure; there is no OH formation and the amount of chemisorbed O remains unchanged for the H_2O exposure at $p(H_2O) = 1 \times 10^{-7}$ Torr and $p(H_2O) = 1 \times 10^{-6}$ Torr; the amount of chemisorbed O decreases slightly with the concomitant formation of a small amount of OH species for H_2O exposure at $p(H_2O) = 1 \times 10^{-5}$ Torr. This indicates that H_2O dissociation at T = 450 °C does not occur for the two lower pressures, and increasing the pressure to $p(H_2O) = 1 \times 10^{-5}$ Torr results in dissociative H_2O adsorption by consuming chemisorbed O, suggesting there is a pressure gap in driving H_2O dissociation.

Figure 5 shows the effect of vapor pressure on the temporal evolution of the intensity ratio of O and OH to the Cu 2p peak for H_2O exposure at T = 100 °C. The first point (i.e., t = 0 min) corresponds to the freshly prepared "29" or "44" oxygenated Cu(111) before H_2O exposure. Chemisorbed O gradually drops to zero at all three pressures and with a faster rate at the higher pressure (Figure 5(a)). OH gradually increases at all three pressures and with a faster rate at the higher pressure, and the amount of OH species at the steady-state decreases as the vapor pressure increases (Figure 5b). Figure 5c shows that the total amount of the oxygen-containing species (O + OH) gradually decreases at all three pressures, and the oxygen-containing species drops faster and more as the vapor pressure increases. The pressure effect on H_2O dissociation is also examined at T = 200, 300, and 450 °C, respectively. The intensity ratio of chemisorbed O and OH to the Cu 2p peak at the steady state is summarized in Table 2 and is plotted in Figure 6 as a function of temperature and vapor pressure. The XPS measurements show that OH species decrease with the temperature increase for the same vapor pressure, and OH also decreases with vapor pressure increase for the same temperature. Meanwhile, chemisorbed O is only partly consumed at T = 300 and 450 °C, indicating that the molecularly adsorbed H_2O becomes less as the temperature increases, which

DOI: 10.1021/acs.jpcc.6b12897
J. Phys. Chem. C 2017, 121, 12117−12126

therefore consumes less chemisorbed O for H_2O dehydrogenation. This is also evidenced from the H_2O exposure at $p(H_2O) = 1 \times 10^{-5}$ Torr and $T = 450$ °C, where the higher vapor pressure leads to some molecularly adsorbed H_2O available for dehydrogenation into OH species by reacting with chemisorbed O that results in a small amount of OH species.

4. DISCUSSION

The results described above show that the clean Cu(111) is nonreactive toward H_2O dissociation; that is, the clean surface is hydrophobic. By contrast, the oxygenated Cu(111) is reactive toward H_2O dissociation which results in the loss of chemisorbed O. From a kinetic point of view, the activation barriers (E_{diss}) for H_2O dissociation on the clean and oxygenated Cu (111) surfaces are different, i.e., E_{diss}(clean) > E_{diss}(oxygenated). The H_2O dissociation barrier for clean Cu(111) was measured to be 1.17 eV from the WGS reaction.[21] This barrier was also proved by other studies in the intermediate pressure region of $p(H_2O) = 1$ Torr and temperature varying from −5 to +60 °C.[20] Also, the linear Brønsted−Evans−Polanyi (BEP) relationship between enthalpy changes and activation energies for water dissociation can be explored to explain why water dissociation is kinetically hindered: the driving force $\Delta H = 0$ (thermoneutral) on clean Cu (111).[41−43]

In contrast, the oxygenated Cu(111) shows reactivity toward H_2O dehydrogenation into OH species by reacting with chemisorbed O. Compared to the freshly prepared oxygenated Cu(111), the overall intensity of the O 1s spectra (including the chemisorbed O and OH components) decreases after reaching the steady state of the H_2O exposure, indicating that more chemisorbed O is consumed than the amount of OH species formed. Mridula et al. reported the reaction sequence of $Cu_2O + H_2O \rightarrow 2CuOH$, $2CuOH \rightarrow 2Cu + H_2 + O_2$ for H_2O dissociation on Cu_2O.[44] The first step of the reaction should result in increased amount of oxygen-containing species (i.e., O and OH) because of the incorporation of additional O from H_2O,[45] i.e.

$$O(ab) + H_2O(g) \rightarrow 2OH(ab) \quad (1)$$

The water molecules can dissociate as the reaction described above is because the reaction barrier for H_2O dissociation is lowered by the chemisorbed O to 0.76 eV.[46] However, as shown from our XPS measurements (Figures 4−6), the total amount of oxygen-containing species (O and OH) decreases after the dehydrogenation reaction. Therefore, additional steps are necessary to remove OH species, i.e., $2OH(ab) \rightarrow H_2(g) + O_2(g)$. The calculation results reported by Chen et al. showed that the direct dissociation of OH species is difficult at both low and high water coverages, but they also reported that OH species can react with another adjacent OH to form O + H_2O.[47] If two OH species combine to form O + H_2O, our entire reaction will be O + $H_2O \rightarrow 2OH \rightarrow O + H_2O$. Therefore, θ_{Total} will either keep constant (if all OH species combine to form O + H_2O) or increase (if partial OH species or no OH species combine to form O + H_2O). Then we introduce the intermediate−peroxo-type (OOH), which is induced through the reaction

$$H_2O(g) + 2O(ab) + OH(ab) \rightarrow OOH(ab) + 2OH(ab) \quad (2)$$

The formation of OOH is only possible on metal surfaces that are covered by chemisorbed O,[48] which is consistent with our experimental results shown above. Then the next step is

$$OOH(ab) + OH(ab) \rightarrow H_2O(g) + O_2(g) \quad (3)$$

Two absorbed O atoms are converted to O_2 after reactions 2 and 3, i.e., $2O(ab) \rightarrow O_2(g)$. If we combine reaction 1 for OH formation with reactions 2 and 3, the entire reaction will be

$$H_2O(g) + 3O(ab) \rightarrow 2OH(ab) + O_2(g) \quad (4)$$

from which three absorbed O atoms are converted to two OH species. This is consistent with the trend shown in our XPS measurements; that is, the total amount of oxygen-containing species decreases upon H_2O exposure.

The continual removal of chemisorbed O atoms will result in only OH groups on the surface, consistent with our experimental results from the H_2O exposure at 100 and 200 °C. The H_2O exposure at 300 °C results in the coexistence of the chemisorbed O and OH species at the steady state and θ_{OH} is much smaller than that for the H_2O exposure at the lower temperatures of 100 and 200 °C. This is because the sticking coefficient of H_2O molecules decreases as the temperature increases, for which there is less molecularly adsorbed H_2O available for the dehydrogenation reaction (and thus less loss of the chemisorbed O). This trend is further confirmed from the H_2O exposure at 450 °C, where barely molecularly adsorbed H_2O is available for dehydrogenation. As a result, the surface does not show loss in chemisorbed O. Meanwhile, it is noticeable that the formation of OOH requires both O and OH species (i.e., step 2). This is why step 1 is necessary to provide OH species at the beginning of the reaction. After the surface is covered by the mixture of O and OH through step 1, absorbed H_2O molecules react with chemisorbed O and neighboring OH to form OOH (step 2). Subsequent reaction step 3 leads to the net loss of chemisorbed O by forming H_2O and O_2 molecules that desorb from the surface at the elevated temperatures. Increasing temperature reduces the amount of molecularly adsorbed H_2O because of the smaller sticking coefficient at a higher temperature, which therefore consumes less amount of chemisorbed O for the H_2O dehydrogenation reaction. This is consistent with the trend that the amount of OH species decreases as temperature increases for the same H_2O vapor pressure (Figure 6b). It can be noted from Figure 6c that the total amount of surface oxygen species (O + OH) increases at 300 and 450 °C because of the significant drop of molecularly adsorbed H_2O, for which chemisorbed O is barely consumed. On the other hand, increasing H_2O vapor pressure results in more molecularly adsorbed H_2O available to react with chemisorbed O, thereby leading to more net loss of surface O. This explains why the total amount of O-containing species (O + OH) decreases with increasing vapor pressure at each temperature (Figure 6c).

It is worthwhile mentioning that XPS detection of the OOH surface species in step 2 is technically challenging because OOH is an unstable surface species.[48−51] In addition, previous studies have showed that OOH is an intermediate during oxygen evolution reduction on various transition metal electrodes but has never been identified spectroscopically.[49−51] However, our experimental result of the required presence of chemisorbed oxygen on the Cu surface for H_2O dissociation points to the formation of OOH as a transient intermediate. This is in line with the previous work that showed that the formation of OOH is only possible on metal surfaces that are

DOI: 10.1021/acs.jpcc.6b12897
J. Phys. Chem. C 2017, 121, 12117−12126

covered by chemisorbed O.[48] To further investigate the feasibility of OOH species on the surface during the reaction, we employed DFT calculations to study the OOH species. We can ignore the OH term in reaction step 2 as it does not react with any other adsorbates and reform and determine if the interaction between H_2O and two chemisorbed oxygen atoms can result in forming OOH. We determined the most stable configurations by varying orientation and adsorption sites for both H_2O molecule and two chemisorbed O atoms, as well as for the OH with OOH on the Cu(111) surface. The two most stable configurations are our initial and final images in our NEB calculation for determining the reaction barriers. Our DFT calculations show that the first H_2O molecule adsorbs on top of a Cu atom on Cu(111) with an adsorption energy of 0.21 eV, which is in good agreement with a previous study of 0.24 eV.[52] Shown in Figure 7a, is the first H_2O, which then interacts with

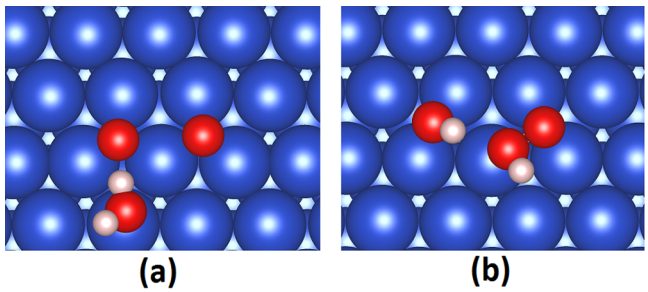

Figure 7. DFT calculations of the interaction of water molecules with chemisorbed O on the Cu(111) surface. (a) The first adsorbed H_2O molecule, (b) OOH formation from H_2O dissociation. The blue balls represent Cu atoms, the red atoms represent O atoms, and the smallest white atoms represent H atoms. The view is perpendicular to the Cu(111) surface.

two nearby chemisorbed O atoms to form OH and OOH species, shown in Figure 7b. One H atom from the H_2O molecule dissociates and adsorbs with a chemisorbed O atom to form OH. The remaining OH from the H_2O molecule then diffuses to the other chemisorbed O atom to form OOH. The energy barrier for this reaction is just 0.17 eV, and the total energy increases by 1.79 eV. The formation of OOH requires a low energy barrier, but the OOH species is not thermodynamically favorable. This suggests that the OOH species is a metastable state that can be formed on an oxygen-covered Cu(111) surface.[53]

5. CONCLUSIONS

The interactions of H_2O molecules on the clean and oxygenated Cu(111) surfaces are comparatively studied with the temperature ranging from 100 to 450 °C and vapor pressure from 1×10^{-7} to 1×10^{-5} Torr. The clean surface does not show reactivity toward H_2O dehydrogenation. By contrast, H_2O dissociates into OH species on the oxygenated Cu(111) by reacting with chemisorbed O. When the temperature is higher than 200 °C, the amount of molecularly adsorbed H_2O available for dehydrogenation decreases, which results in a smaller amount of OH species and less loss of chemisorbed O. The dehydrogenation of molecularly adsorbed H_2O is suggested to proceed via a three-step reaction pathway that results in the net loss of chemisorbed oxygen from the surface, (1) $H_2O(g) + O(ab) \rightarrow 2OH(ab)$, (2) $H_2O(g) + OH(ab) + 2O(ab) \rightarrow OOH(ab) + 2OH(ab)$, followed by (3) $OOH(ab) + OH(ab) \rightarrow H_2O(g) + O_2(g)$, in which the formation of OOH species is not directly demonstrated in the experiments but is supported by DFT calculations. These results provide insight into understanding the elemental steps of the dehydrogenation of H_2O molecules and may find broader applicability for tuning the surface reactivity toward H_2O dehydrogenation for catalytic gas-surface reactions in which H_2O dissociation is involved.

■ ASSOCIATED CONTENT

Supporting Information

The Supporting Information is available free of charge on the ACS Publications website at DOI: 10.1021/acs.jpcc.6b12897.

C 1s XPS spectra showing that there is no carbon contamination for the freshly cleaned surface and after the O_2 and H_2O exposures. (PDF)

■ AUTHOR INFORMATION

Corresponding Author

*E-mail: gzhou@binghamton.edu.

ORCID

Guangwen Zhou: 0000-0002-9243-293X

Notes

The authors declare no competing financial interest.

■ ACKNOWLEDGMENTS

We acknowledge the support by National Science Foundation under NSF CAREER Award Grant CMMI-1056611 and CBET-1264940. Research in part was carried out in the Center for Functional Nanomaterials, Brookhaven National Laboratory, which is supported by the U.S. Department of Energy, Office of Basic Energy Sciences, under Contract No. DE-AC02-98CH10886.

■ REFERENCES

(1) Demirci, E.; Stettner, J.; Kratzer, M.; Schennach, R.; Winkler, A. Methanol Adsorption on Cu(110) and the Angular Distribution of the Reaction Products. *J. Chem. Phys.* **2007**, *126*, 164710.

(2) Shustorovich, E.; Bell, A. T. Oxygen-Assisted Cleavage of O-H, N-H, and C-H Bonds on Transition Metal Surfaces: Bond-Order-Conservation-Morse-Potential Analysis. *Surf. Sci.* **1992**, *268*, 397−405.

(3) Afsin, B.; Davies, P. R.; Pashusky, A.; Roberts, M. W.; Vincent, D. Reaction Pathways in the Oxydehydrogenation of Ammonia at Cu(110) Surfaces. *Surf. Sci.* **1993**, *284*, 109−120.

(4) Boronin, A.; Pashusky, A.; Roberts, M. W. A New Approach to the Mechanism of Heterogeneously Catalysed Reactions: The Oxydehydrogenation of Ammonia at a Cu(111) Surface. *Catal. Lett.* **1992**, *16*, 345−350.

(5) Sexton, B. A.; Hughes, A. E.; Avery, N. R. Spectroscopic Study of the Adsorption and Reactions of Methanol, Formaldehyde and Methyl Formate on Clean and Oxygenated Cu(110) Surfaces. *Surf. Sci.* **1985**, *155*, 366−386.

(6) Chen, H.-T.; Choi, Y.; Liu, M.; Lin, M. C. A First-Principles Analysis for Sulfur Tolerance of CeO2 in Solid Oxide Fuel Cells. *J. Phys. Chem. C* **2007**, *111*, 11117−11122.

(7) Au, C.-T.; Roberts, M. W. The Promotion of Surface-Catalysed Reactions by Gaseous Additives. The Role of a Surface Oxygen Transient. *J. Chem. Soc., Faraday Trans. 1* **1987**, *83*, 2047−2059.

(8) Davis, J. L.; Barteau, M. A. Reactions of Carboxylic Acids on the Pd(111)-(2 × 2)O Surface: Multiple Roles of Surface Oxygen Atoms. *Surf. Sci.* **1991**, *256*, 50−66.

(9) Stuve, E. M.; Madix, R. J. Oxidation of Ethylene on Pd(100); Bonding of Ethylene and Scavenging of Dehydrogenation Fragments by Surface Oxygen. *Surf. Sci.* **1985**, *160*, 293−304.

(10) Davis, S. M.; Somorjai, G. A. The Effect of Surface Oxygen on Hydrocarbon Reactions Catalyzed by Platinum Crystal Surfaces with Variable Kink Concentrations. *Surf. Sci.* **1980**, *91*, 73−91.
(11) Tagawa, H.; Endo, T. Catalytic Decomposition of Sulfuric Acid Using Metal Oxides as the Oxygen Generating Reaction in Thermochemical Water Splitting Process. *Int. J. Hydrogen Energy* **1989**, *14*, 11−17.
(12) Wei, X.; Dong, C.; Chen, Z.; Xiao, K.; Li, X. A DFT Study of the Adsorption of O_2 and H_2O on Al(111) Surfaces. *RSC Adv.* **2016**, *6*, 56303−56312.
(13) Jiang, J.; Li, M.; Yan, Y.; Fang, T. Decomposition of H_2O on Clean and Oxygen-Covered Au(100) Surface: A DFT Study. *Appl. Surf. Sci.* **2014**, *315*, 16−21.
(14) Wang, W.; Wang, G.; SHao, M. First-Principles Modeling of Direct versus Oxygen-Assisted Water Dissociation on Fe(100) Surfaces. *Catalysts* **2016**, *6*, 29.
(15) Wang, Y. Q.; Yan, L. F.; Wang, G. C. Oxygen Assisted Water Partial Dissociation on Copper: a Model Study. *Phys. Chem. Chem. Phys.* **2015**, *17*, 8231−8238.
(16) Liu, P. Water-Gas Shift Reaction on Oxide/Cu(111): Rational Catalyst Screening from Density Functional Theory. *J. Chem. Phys.* **2010**, *133*, 204705.
(17) Nakamura, J.; Campbell, J. M.; Campbell, C. T. Kinetics and Mechanism of the Water-Gas Shift Reaction Catalysed by the Clean and Cs-Promoted Cu(110) Surface: A Comparison with Cu(111). *J. Chem. Soc., Faraday Trans.* **1990**, *86*, 2725−2734.
(18) Campbell, C. T.; Koel, B. E.; Daube, K. A. Surface Science Studies of the Water−Gas Shift Reaction on a Model Cu(111) Catalyst. *J. Vac. Sci. Technol., A* **1987**, *5*, 810−813.
(19) Gokhale, A. A.; Dumesic, J. A.; Mavrikakis, M. On the Mechanism of Low-Temperature Water Gas Shift Reaction on Copper. *J. Am. Chem. Soc.* **2008**, *130*, 1402−1414.
(20) Yamamoto, S.; Andersson, K.; Bluhm, H.; Ketteler, G.; Starr, D. E.; Schiros, T.; Ogasawara, H.; Pettersson, L. G. M.; Salmeron, M.; Nilsson, A. Hydroxyl-Induced Wetting of Metals by Water at near-Ambient Conditions. *J. Phys. Chem. C* **2007**, *111*, 7848−7850.
(21) Campbell, C. T.; Daube, K. A. A Surface Science Investigation of the Water-Gas Shift Reaction on Cu(111). *J. Catal.* **1987**, *104* (1), 109−119.
(22) Jensen, F.; Besenbacher, F.; Laegsgaard, E.; Stensgaard, I. Oxidation of Cu(111): Two New Oxygen Induced Reconstructions. *Surf. Sci.* **1991**, *259*, L774−L780.
(23) Jensen, F.; Besenbacher, F.; Stensgaard, I. Two New Oxygen Induced Reconstructions on Cu(111). *Surf. Sci.* **1992**, *269-270*, 400−404.
(24) Matsumoto, T.; Bennett, R. A.; Stone, P.; Yamada, T.; Domen, K.; Bowker, M. Scanning Tunneling Microscopy Studies of Oxygen Adsorption on Cu(111). *Surf. Sci.* **2001**, *471* (1−3), 225−245.
(25) Yang, F.; Choi, Y. M.; Liu, P.; Hrbek, J.; Rodriguez, J. A. Autocatalytic Reduction of a Cu2O/Cu(111) Surface by CO: STM, XPS, and DFT Studies. *J. Phys. Chem. C* **2010**, *114*, 17042−17050.
(26) Therrien, A. J.; Zhang, R.; Lucci, F. R.; Marcinkowski, M. D.; Hensley, A.; McEwen, J.-S.; Sykes, E. C. H. Structurally Accurate Model for the "29"-Structure of CuxO/Cu(111): A DFT and STM Study. *J. Phys. Chem. C* **2016**, *120* (20), 10879−10886.
(27) Kresse, G.; Furthmuller, J. Efficient Iterative Schemes for Ab Initio Total-Energy Calculations Using a Plane-Wave Basis Set. *Phys. Rev. B: Condens. Matter Mater. Phys.* **1996**, *54* (16), 11169−11186.
(28) Kresse, G.; Furthmuller, J. Efficiency of Ab-Initio Total Energy Calculations for Metals and Semiconductors Using a Plane-Wave Basis Set. *Comput. Mater. Sci.* **1996**, *6*, 15−50.
(29) Perdew, J. P.; Chevary, J. A.; Vosko, S. H.; Jackson, K. A.; Pederson, M. R.; Singh, D. J.; Fiolhais, C. Atoms, Molecules, Solids, and Surfaces: Applications of the Generalized Gradient Approximation for Exchange and Correlation. *Phys. Rev. B: Condens. Matter Mater. Phys.* **1992**, *46* (11), 6671−6687.
(30) Blochl, P. E. Projector Augmented-Wave Method. *Phys. Rev. B: Condens. Matter Mater. Phys.* **1994**, *50* (24), 17953−17979.
(31) Kresse, G.; Joubert, D. From Ultrasoft Pseudopotentials to the Projector Augmented-Wave mMethod. *Phys. Rev. B: Condens. Matter Mater. Phys.* **1999**, *59* (3), 1758−1775.
(32) Monkhorst, H. J.; Pack, J. D. On Special Points for Brillouin-Zone Integrations. *Phys. Rev. B* **1976**, *13*, 5188−5192.
(33) Li, L.; Xi, M.; Shi, Y. F.; Zhou, G. W. Precursor to the Bulk Oxide Formation during the Oxidation of Cu(100). *Phys. Rev. Lett.* **2012**, *108*, 176102.
(34) Li, L.; Zhou, G. W. Oxygen Subsurface Adsorption on the Cu(110)-c(6 × 2) Surface. *Surf. Sci.* **2013**, *615*, 57−64.
(35) Li, J.; Zhou, G. W. Density Functional Theory Study of O−H and C−H Bond Scission of Methanol Catalyzed by a Chemisorbed Oxygen Layer on Cu(111). *Surf. Sci.* **2016**, *646*, 288−297.
(36) Li, J.; Li, L.; Zhou, G. W. The Onset of Sub-Surface Oxidation Induced by Defects in a Chemisorbed Oxygen Layer. *J. Chem. Phys.* **2015**, *142*, 084701.
(37) Henkelman, G.; Uberuaga, B. P.; Jónsson, H. A Climbing Image Nudged Elastic Band Method for Finding Saddle Points and Minimum Energy Paths. *J. Chem. Phys.* **2000**, *113*, 9901−9904.
(38) Momma, K.; Izumi, F. VESTA: A Three-Dimensional Visualization System for Electronic and Strucural Analysis. *J. Appl. Crystallogr.* **2008**, *41*, 653−658.
(39) Poulston, S.; Parlett, P. M.; Stone, P.; Bowker, M. Surface Oxidation and Reduction of CuO and Cu_2O Studied Using XPS and XAES. *Surf. Interface Anal.* **1996**, *24*, 811−820.
(40) Dahlang, T.; Sven, T. Electronic and Optical Properties of Cu, CuO and Cu_2O Studied by Electron Spectroscopy. *J. Phys.: Condens. Matter* **2012**, *24*, 175002.
(41) Michaelides, A.; Alavi, A.; King, D. A. Insight into H_2O-Ice Adsorption and Dissociation on Metal Surfaces from First-Principles Simulations. *Phys. Rev. B: Condens. Matter Mater. Phys.* **2004**, *69*, 113404.
(42) Kandoi, S.; Gokhale, A. A.; Grabow, L. C.; Dumesic, J. A.; Mavrikakis, M. Why Au and Cu Are More Selective Than Pt for Preferential Oxidation of Co at Low Temperature. *Catal. Lett.* **2004**, *93*, 93−100.
(43) Michaelides, A.; Liu, Z. P.; Zhang, C. J.; Alavi, A.; King, D. A.; Hu, P. Identification of General Linear Relationships between Activation Energies and Enthalpy Changes for Dissociation Reactions at Surfaces. *J. Am. Chem. Soc.* **2003**, *125*, 3704−3705.
(44) Bharadwaj, M. D.; Yang, J. C. The Reduction of Cu_2O by Water Vapor. *Scr. Mater.* **2001**, *44*, 2557−2561.
(45) Henderson, M. A. The Interaction of Water with Solid Surfaces: Fundamental Aspects Revisited. *Surf. Sci. Rep.* **2002**, *46* (1−8), 1−308.
(46) Wang, G.-C.; Tao, S.-X.; Bu, X.-H. A Systematic Theoretical Study of Water Dissociation on Clean and Oxygen-Preadsorbed Transition Metals. *J. Catal.* **2006**, *244*, 10−16.
(47) Chen, L.; Zhang, Q.; Zhang, Y.; Li, W. Z.; Han, B.; Zhou, C.; Wu, J.; Forrey, R. C.; Garg, D.; Cheng, H. A First Principles Study of Water Dissociation on Small Copper Clusters. *Phys. Chem. Chem. Phys.* **2010**, *12*, 9845−9851.
(48) Rossmeisl, J.; Logadottir, A.; Nørskov, J. K. Electrolysis of Water on (Oxidized) Metal Surfaces. *Chem. Phys.* **2005**, *319*, 178−184.
(49) Yeo, B. S.; Klaus, S. L.; Ross, P. N.; Mathies, R. A.; Bell, A. T. Identification of Hydroperoxy Species as Reaction Intermediates in the Electrochemical Evolution of Oxygen on Gold. *European Journal of Chemical Physics and Physical Chemistry* **2010**, *11*, 1854−1857.
(50) Lyons, M. E.; Brandon, M. P. The Oxygen Evolution Reaction on Passive Oxide Covered Transition Metal Electrodes in Alkaline Solution Part II - Cobalt. *Int. J. Electrochem. Sci.* **2008**, *3*, 1425−1462.
(51) Damjanovic, A.; Dey, A.; Bockris, J. O. M. Kinetics of Oxygen Evolution and Dissolution on Platinum Electrodes. *Electrochim. Acta* **1966**, *11*, 791−814.
(52) Michaelides, A.; Ranea, V. A.; de Andres, P. L.; King, D. A. General Model for Water Monomer Adsorption on Close-Packed Transition and Noble Metal Surfaces. *Phys. Rev. Lett.* **2003**, *90*, 216102.
(53) As noted by one reviewer, the instability of OOH may be attributed to the large difference in electronegativity between Cu and

DOI: 10.1021/acs.jpcc.6b12897
J. Phys. Chem. C 2017, 121, 12117−12126

O. The oxidation of the more negatively charged O and OH to the less negatively charged OOH would normally only occur under electrochemical and photochemical conditions.

DOI: 10.1021/acs.jpcc.6b12897
J. Phys. Chem. C 2017, 121, 12117−12126